

Article

Zr as an Alternative Grain Refiner in the Novel AlSi5Cu2Mg Alloy

Dana Bolibruchová ¹, Marek Matejka ^{1,*}, Lukáš Širanec ¹ and Martin Švec ²

¹ Department of Technological Engineering, Faculty of Mechanical Engineering, University of Žilina, Univerzitná 8215/1, 010 26 Žilina, Slovakia; danka.bolibruchova@fstroj.uniza.sk (D.B.); lukas.siranec@fstroj.uniza.sk (L.Š.)

² Department of Engineering Technology, Faculty of Mechanical Engineering, Technical University of Liberec, Studentská 1402/2, 461 17 Liberec, Czech Republic; martin.svec@tul.cz

* Correspondence: marek.matejka@fstroj.uniza.sk; Tel.: +421-41-513-2771

Abstract: Al-Si-Cu-Mg alloys are among the most significant types of aluminum alloys, accounting for 85–90% of all castings used in the automotive sector. These alloys are used, for example, in the manufacturing of engine blocks and cylinder heads due to their excellent specific strength (ratio of strength to specific weight) and superior castability and thermal conductivity. This study investigated the effect of using Zr as an alternative grain refiner in the novel AlSi5Cu2Mg cylinder head alloy. The microstructure of this alloy could not be refined via common Al-Ti-B grain refiners due to its specifically designed chemical composition, which limits the maximum Ti content to 0.03 wt.%. The results showed that the addition of Zr via the AlZr20 master alloy led to a gradual increase in the solidus temperature and to the grain refinement of the microstructure with the addition of as little as 0.05 wt.% Zr. The addition of more Zr (0.10, 0.15, and 0.20 wt.%) led to a gradual grain refinement effect for the alloy. The presence of Zr in the AlSi5Cu2Mg alloy was reflected in the formation of Zr-rich intermetallic phases with acicular morphology. Such phases acted as potent nucleants for the α -Al grain.

Keywords: zirconium; grain refinement; AlSi5Cu2Mg; microstructure; thermal analysis



Citation: Bolibruchová, D.; Matejka, M.; Širanec, L.; Švec, M. Zr as an Alternative Grain Refiner in the Novel AlSi5Cu2Mg Alloy. *Metals* **2024**, *14*, 581. <https://doi.org/10.3390/met14050581>

Academic Editor: Maciej Motyka

Received: 3 April 2024

Revised: 27 April 2024

Accepted: 13 May 2024

Published: 15 May 2024



Copyright: © 2024 by the authors. Licensee MDPI, Basel, Switzerland. This article is an open access article distributed under the terms and conditions of the Creative Commons Attribution (CC BY) license (<https://creativecommons.org/licenses/by/4.0/>).

1. Introduction

Over the years, Al-Si cast alloys have found extensive applications, especially in the automotive industry. This sector has undergone significant changes in recent years, mainly due to increasingly strict environmental requirements [1–4]. Closely related to this change is the need to improve the utility properties of Al-Si cast aluminum alloys to achieve a weight reduction in car components and an associated reduction in CO₂ emissions from cars. Optimizing the chemical composition of Al-Si cast alloys, heat treatments, or metallurgical operations (grain refinement, eutectic Si modification) are among the basic methods used to increase the utility properties of aluminum alloys [5–8]. Grain refinement, with the aim of obtaining a uniform and fine texture, is common practice in commercial production. Grain refinement can have a significant effect, mainly on the mechanical properties of hypoeutectic Al-Si alloys, but also on subsequent deformation processes. As a result of the addition of the grain refiner, the grain size of α -Al can be significantly reduced, creating more grain boundaries that can act as insurmountable borders for dislocation movements, resulting in an increase in the yield strength of the material [9–15].

Nucleation theory states that, while adequate effective solutes provide undercooling that encourages the nucleation of neighboring nucleant particles during the solidification of Al alloys, a large number of potent nucleants facilitate α -Al nucleation with little undercooling [16]. Based on the current research, nucleate potency in grain refinement can be classified into two categories. According to one theory, coherent crystallographic orientation should reduce the interfacial energy between the nuclei and the matrix in an efficient

nucleate. A different approach, the free-growth model, places more emphasis on the size of the nuclei particles and suggests that, in order for the nucleation to proceed properly, an efficient nucleus particle should be larger than a crucial threshold value [16–19].

Grain refiner is added to the aluminum alloy during the chemical process, which primarily refines the grain. Al–Ti–B and Al–Ti–C systems have previously been studied, since they are the most widely used Al alloy grain refiners in industrial manufacturing. However, several studies [20–24] have found that zirconium can also effectively reduce the grain size of Al–Si alloys. According to these studies, the grain-refining effect of Zr can be attributed to the peritectic reaction induced by the pro-peritectic Al_3Zr phase, which acts as a potent nucleation site for α -Al grains. Potential nucleating particles such as pro-peritectic Al_3Zr compounds have previously been studied for their heterogeneous nucleation on nuclei particles, crystallography, and particle size distribution. The pro-peritectic Al_3Zr particles have been discovered to have a high potency as efficient nuclei due to their favorable crystallographic matching and consistent orientation associations with the Al matrix. Additionally, a size–distribution analysis of pro-peritectic Al_3Zr particles has been performed. The outcomes were in good agreement with the concept of free growth. This suggests that a portion of the pro-peritectic Al_3Zr particles generated in situ may be sized appropriately to encourage heterogeneous nucleation [25,26].

The advantage of the presence of zirconium (Zr) in aluminum alloys is that it causes the formation of a thermally stable dispersion phase. Zirconium particles are resistant to coarsening due to their low matrix interface energy, which limits the diffusion and solubility of rate-affecting elements. This predisposes Zr-alloyed alloys for use at elevated temperatures [27]. In general, the addition of Zr to the alloy increases its strength properties and hardness. Even a small amount of Zr increases the hardness of the finished product due to the formation of the Al_3Zr phase, which increases not only the hardness, but also the wear resistance of the material [28].

The aging-strengthening ability and thermal stability of aluminum alloys below 400 °C can be improved by the presence of metastable Al_3Zr precipitates with an L_{12} cubic structure. Nonetheless, the low solubility of Zr in Al (660 °C: 0.28%) and its diffusivity (400 °C: $1.2 \times 10^{-20} \text{ m}^2 \cdot \text{s}^{-1}$) cause coarse primary Al_3Zr particles to precipitate easily in the Zr-containing aluminum alloys. Due to their strong thermal durability, the primary Al_3Zr particles have difficulty dissolving during the homogenization process. Because primary Al_3Zr reduces Zr saturation in Al, it weakens Zr's ability to strengthen Al. As a result, the characteristics of Zr-containing aluminum alloys are affected. Therefore, in these types of aluminum alloys, it is imperative to prevent the development of coarse primary Al_3Zr [29,30].

The present study evaluated the effect of a Zr-based grain refiner on the microstructure of the AlSi5Cu2Mg alloy. This alloy has a chemical composition specifically designed by its manufacturer, whereby the Ti content is limited to max. 0.03 wt.%. For this reason, commonly used grain refiners based on Al–Ti–B cannot be used to refine the microstructure of this alloy. Therefore, our goal was to find a suitable grain refiner that would refine the grain structure of the AlSi5Cu2Mg alloy and replace the standard Al–Ti–B-based grain refiner.

2. Materials and Methods

The hypoeutectic AlSi5Cu2Mg aluminum alloy was used in this study. This alloy is currently used for the production of cylinder head castings for a Korean automotive concern. As it is a relatively new alloy, there are no scientific studies on its microstructure or crystallization process or on the impact of the addition of Zr on the grain refinement of this alloy.

To study the impact of Zr, five AlSi5Cu2Mg aluminum alloys with different levels of added Zr (0; 0.05; 0.10; 0.15; and 0.20 wt.%) were produced. The chemical composition of these alloys (obtained via arc spectroscopy) is given in Table 1. The experimental alloys were made using gravity casting in an open atmosphere. The batch material was prepared

in the form of ingots, which were cut to the required size before melting. Each batch had a weight of 10 kg. Melting was carried out in an electric resistance furnace with a T15-type regulator with a capacity of 15 kg in a graphite crucible that was treated with a protective coating. Before each casting, oxide films were mechanically removed from the surface of the melt. It was cast into a permanent mold at a temperature of 200 ± 10 °C. The casting temperature was set to 770 °C. Zirconium was added to the AlSi5Cu2Mg alloy melt in the form of the AlZr20 master alloy. The master alloy and the AlSi5Cu2Mg alloy ingots were supplied by a foundry that produces cylinder head castings for a Korean automotive concern. A microstructural evaluation was performed on the experimental alloys in an as-cast state.

Table 1. Chemical composition of the experimental alloys.

Zr Addition (wt.%)	Si	Cu	Mg	Fe	Mn	Ti	Sr	Zr	Al
0	5.47	1.91	0.29	0.18	0.02	0.013	0.01	0.0009	Bal.
0.05	5.67	1.91	0.29	0.19	0.02	0.013	0.01	0.05	Bal.
0.10	5.65	1.92	0.29	0.19	0.02	0.014	0.01	0.10	Bal.
0.15	5.55	1.91	0.29	0.19	0.02	0.014	0.01	0.12	Bal.
0.20	5.43	1.90	0.29	0.18	0.02	0.014	0.01	0.19	Bal.

The NEOPHOT 32 optical microscope was used for light optical microscopy when assessing the samples' microstructures (Carl Zeiss, Jena, Germany), while the Oxford UltimMax 65 electron microscope (Oxford Instruments, Abingdon, UK) was used for scanning electron microscopy (SEM). Standard metallographic techniques (coarse and fine wet grinding, polishing on an automatic machine using diamond emulsion, and etching) were used to prepare the samples for the microstructural investigation. In order to use light microscopy, the samples were etched with 20 mL of H₂SO₄ and 100 mL of distilled water to emphasize the Zr-rich phases. Using a 0.5% HF solution, the samples used for SEM and energy-dispersive X-ray spectroscopy (EDS) analysis were etched.

The grain size of the experimental alloys was determined using EBSD analysis on a Tescan Mira 3 microscope supplemented (Brno, Czech Republic) with an Oxford Symmetry EBSD detector (Oxford Instruments, Abingdon, UK). Microscopical observations were made using a SEM microscope TESCAN LMU II with a BRUKER EDX analyzer (Billerica, MA, USA).

The solidification of the experimental alloys was recorded via a thermal analysis. The measuring device consisted of a K-type thermocouple placed in a cylindrical metal mold with a diameter of 35 mm and a height of 55 mm. Using LabView 2 Hz software (version 18.5, National Instruments, Austin, TX, USA), the temperature dependence on time for the alloy during solidification in the mold was recorded. With the help of the measured curve and its first derivative, the characteristic temperatures of formation of the individual structural components of the reference alloy were subsequently determined. The given values represent the temperatures at which the crystallization of the individual structural components began.

Two thermocouples were used to determine the point of dendritic coherence and the lowest temperature difference. This technique was developed by Backerud [31]. One thermocouple is placed in the center of a cylindrical mold and the other is placed on the wall. An additional phase begins to form at the wall of the mold and moves toward the center as solidification progresses. As a result, the latent heat of solidification is released near the mold wall rather than at the center of the mold. The difference in temperature between the two thermocouples is noted. Initially, while the area surrounding the thermocouple in the core of the mold is still in the liquid phase, solidification can increase the temperature of the thermocouple located at the mold wall. This is when the temperature difference curve begins to rise. The temperature differential curve will decrease to a minimum value as the

heat wave gradually moves from the mold wall to the core. At this point, the primary phase of nucleation is complete. The temperature curve then begins to rise again. This is known as the DCP, the point at which the temperature difference curve reaches its minimum value.

Twenty millimeters from the bottom of the crucible in the melt, one thermocouple is positioned exactly in the center of the crucible (T_C) and the other is positioned very close to the inner wall (T_W). The DCP is calculated by plotting the ΔT curve in each experiment and calculating the temperature difference between the wall and core regions during solidification according to Equation (1):

$$\Delta T = T_W - T_C \quad (1)$$

The microhardness measurement was carried out using a Hanemann microhardness tester type Mod 32 (Jena, Germany). The device uses the Vickers method, and the advantage of this hardness tester is that it allows for the direct measurement of the created imprints. In total, 10 imprints were performed for each structure evaluated.

3. Results

3.1. Microstructure

The microstructure of the reference alloy AlSi5Cu2Mg is formed by dendrites of the α -Al phase, eutectic Si in a modified state, and intermetallic phases based on Cu, Mg, and Fe (Figure 1). By modifying the eutectic silicon, a change in morphology was achieved from the original plate-like structure to a rod-like or fibrous structure, which is observed as imperfectly round grains in the plane of the cut. Intermetallic phases rich in Cu were excluded (reference alloy) in the form of oval particles, represented as a ternary eutectic Al-Al₂Cu-Si in the form of compact formations. Their crystallization took place near the needles of the iron-based phases or isolated between the dendrites of the α -Al phase. Iron-rich intermetallic phases were observed in the reference alloy preferentially in the acicular β -Al₅FeSi morphology (Figure 1b).

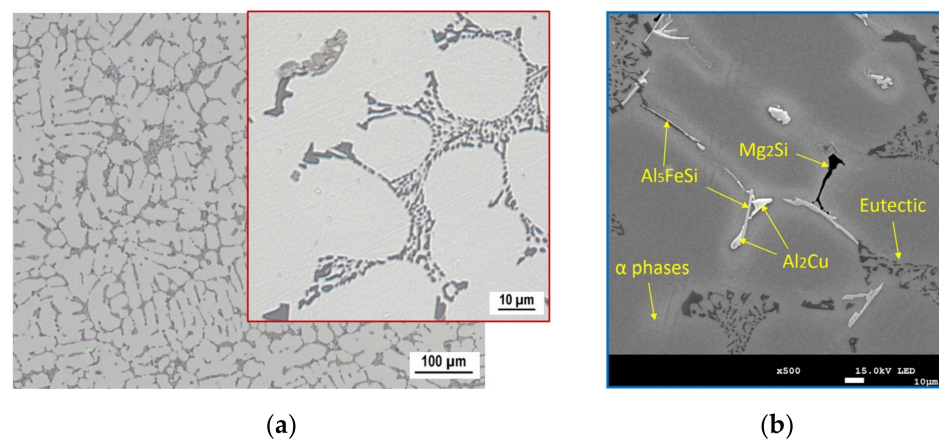


Figure 1. Microstructure of the reference alloy AlSi5Cu2Mg without added Zr (etch, H₂SO₄): (a) optical microscope images representing the character of the microstructure; (b) SEM images with a description of individual structural components.

The character of the experimental AlSi5Cu2Mg alloys' microstructure did not change significantly with the graded addition of Zr when compared to the reference alloy (Figure 2). The microstructures are formed by the α -Al phase, modified eutectic Si, intermetallic phases based on Cu, Mg, and Fe, and the presence of phases rich in Zr. Intermetallic phases rich in copper were separated in the form of oval grains of an Al-Al₂Cu-Si ternary eutectic. The presence of Mg in the microstructure mainly manifested in the formation of a complex phase based on Al-Fe-Mg-Si in the form of sharp-edged grains. Phases rich in iron were present in all of the experimental alloys in the needle-like morphology of β -Al₅FeSi, or,

together with manganese, it formed a complex phase of the $\text{Al}_{15}(\text{FeMn})_3\text{Si}_2$ type with a morphology in the form of a segmented Chinese script.

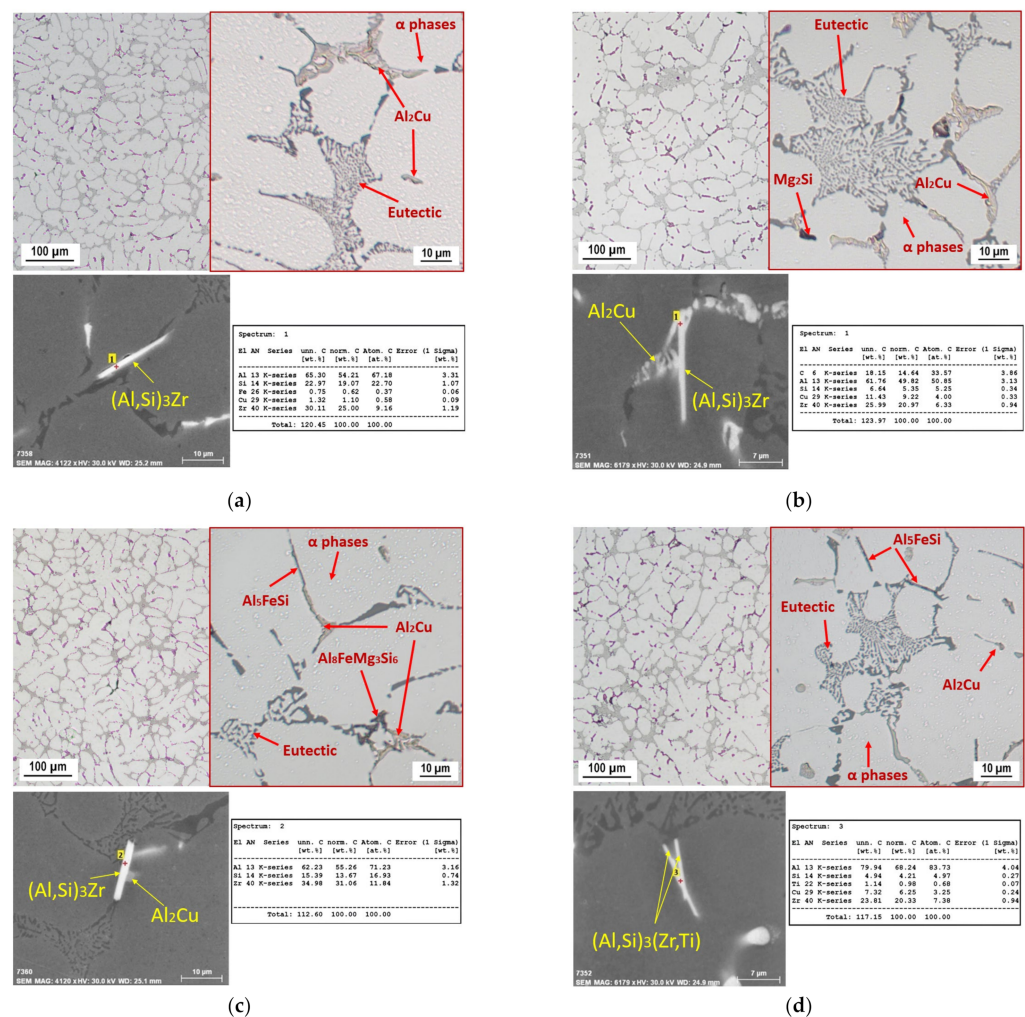


Figure 2. Microstructures of the experimental $\text{AlSi}_5\text{Cu}_2\text{Mg}$ alloys with the graded addition of Zr (etch, H_2SO_4); optical microscope images representing the character of the microstructure; SEM-point EDX analysis focused on Zr-rich phases: (a) addition of 0.05 wt.% Zr; (b) addition of 0.10 wt.% Zr; (c) addition of 0.15 wt.% Zr; (d) addition of 0.20 wt.% Zr.

The addition of Zr in the range of 0.05–0.20 wt.% in the $\text{AlSi}_5\text{Cu}_2\text{Mg}$ alloy caused the formation of intermetallic phases rich in Zr with a needle-like morphology (Figure 2: SEM images with point EDX analysis). These are primarily phases based on Al_3Zr , which were also observed in $(\text{Al,Si})_3\text{Zr}$ and $(\text{Al,Si})_3(\text{Zr,Ti})$, together with the content of Si elements, respectively, Ti and Cu, the phases of which are crystallized in close proximity. Such phases are crystallized either as single needles (Figure 2a–c) or as a cluster of two crossed needles (Figure 2d). Their length was not affected by the amount of Zr added, and ranged from 14 to 19 μm . As the amount of Zr increased, an increase in their number in the microstructure was observed without a change in morphology.

Phases based on Al-Zr in the experimental alloys are present in the stable tetragonal ($D0_{22}$) system, as it was formed directly from the melt during solidification. It is predominant to notice that the needle morphology negatively affects the homogeneity of the microstructure, since the sharp ends of the needles act as stress concentrators in the alloy. On the other hand, the presence of the Al_3Zr (resp., $(\text{Al,Si})_3\text{Zr}$ and $(\text{Al,Si})_3(\text{Zr,Ti})$) phase hinders the movement of a dislocation, which increases the stress of the crystal slip and the density of the dislocations, leading to enhanced mechanical properties. Likewise, Al_3Zr

acts as a hard particle in the aluminum matrix, which reduces the tendency to abrasive wear by providing resistance to deformation [32].

3.2. Crystallization Process

The crystallization of the reference alloy AlSi5Cu2Mg (Figure 3a) started at 615 °C with the formation of the primary α -Al phase. The solidification of the alloy continued with the crystallization of the eutectic phase at a temperature of 565 °C. The beginning of the crystallization of Mg-rich intermetallic phases (identified as Mg₂Si) was identified from the cooling curve and its first derivative at a temperature of 555 °C. The crystallization of the intermetallic phases of the Al₂Cu type began at a temperature of 543 °C. The solidification of the alloy was completed by reaching the solidus temperature of 517 °C. Figure 3b shows a comparison of the cooling curves and their first derivatives and the reference alloy with 0.2 wt.% Zr.

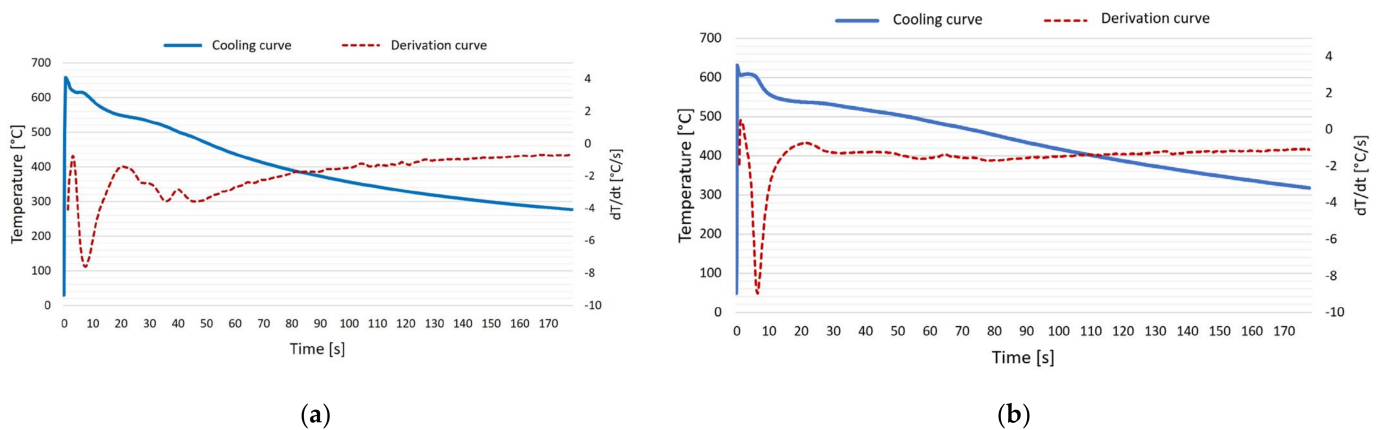


Figure 3. Cooling curve and first derivative: (a) reference alloy AlSi5Cu2Mg; (b) AlSi5Cu2Mg with the addition of 0.20 wt.% Zr.

As the amount of added Zr increased, the temperature of the liquid also increased, while the highest temperature ($T_{liq} = 621$ °C) was reached in the experimental alloy with an addition of 0.20 wt.% Zr. Together with Zr, Al crystallized into the Al₃Zr ((Al,Si)₃Zr or (Al,Si)₃(Zr,Ti)) phase in the tetragonally stable D0₂₂ crystallographic system, which is formed as a primary phase by crystallization directly from the melt during solidification [30]. Based on the created cooling curves and their first derivatives, it was determined that the characteristic temperatures of the phase transformations of the eutectic phase and intermetallic phases rich in Mg and Cu were not affected by the rapid increase in Zr in the alloy. The crystallization of the eutectic phase in the experimental alloys ranged from 564 to 568 °C, Mg-rich phases from 552 to 557 °C, and Cu-rich phases from 540 to 545 °C. The increase in the temperature of the liquid after the addition of Zr influenced the expansion of the experimental alloys' solidification intervals, which could also be related to, e.g., the higher susceptibility of the experimental alloys to the formation of cracks or shrinkage. Alloying the AlSi5Cu2Mg alloy with the graded addition of Zr had an effect on the temperature of the liquidus T_{liq} , but the temperature of the solidus T_{sol} remained constant (Table 2).

Table 2. Liquidus and solidus temperatures of the experimental alloys.

Zr Addition (wt.%)	T_{liq} (°C)	T_{sol} (°C)
0	615	517
0.05	617	518
0.10	618	518
0.15	620	517
0.20	621	518

A detailed examination of the cooling curve around liquid temperatures shows a change in the undercooling below the equilibrium temperature ΔT_L and the size of the recalescence ΔT_L (Figure 4). As the amount of Zr increases, the value of undercooling below the equilibrium temperature decreases along with recalescence, which causes an improvement in the condition of the crystallization nuclei of the primary phase.

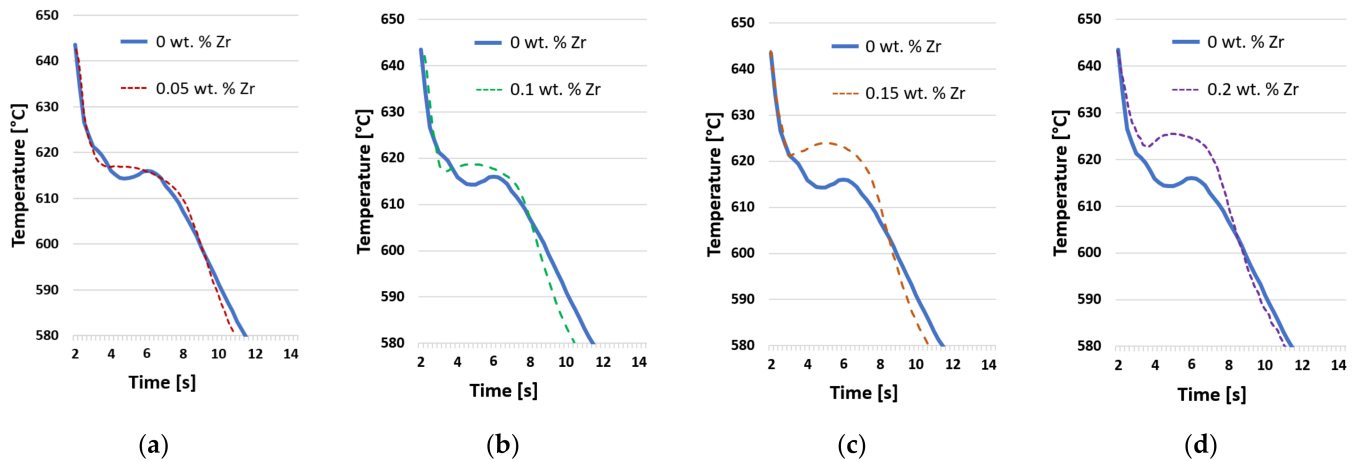


Figure 4. Cooling curve in the area of liquid temperatures compared to the reference alloy AlSi5Cu2Mg: (a) addition of 0.05 wt.% Zr; (b) addition of 0.10 wt.% Zr; (c) addition of 0.15 wt.% Zr; (d) addition of 0.20 wt.% Zr.

The improvement of the condition of the crystallization nuclei of the primary phase led to the effective seeding effect of the Zr element on the AlSi5Cu2Mg alloy, which confirmed the results obtained using EBSD in our previous research (Figure 5) [33]. The EBSD results showed a 53% decrease in grain size (0 wt.% Zr: 510 μm ; 0.20 wt.% Zr: 240 μm). This indicates that the addition of Zr resulted in the formation of Zr-rich intermetallic phases, which acted as potent nucleants for Al.

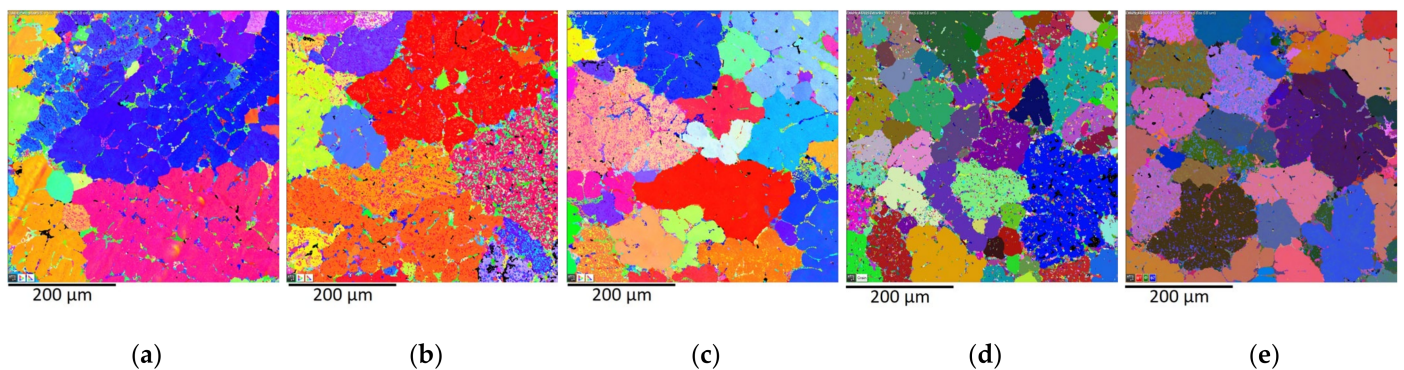


Figure 5. EBSD images of the experimental AlSi5Cu2Mg alloys, depending on the amount of Zr added: (a) 0 wt.% Zr (without addition); (b) addition of 0.05 wt.% Zr; (c) addition of 0.10 wt.% Zr; (d) addition of 0.15 wt.% Zr; (e) addition of 0.20 wt.% Zr.

The intermetallic phases formed could act as strong nuclei for α -Al in the AlSi5Cu2Mg alloy via two main mechanisms. The existing research shows that a potential grain refiner element in aluminum alloys should have a partition coefficient k_0 greater than 1 so that it is preferentially absorbed by the emerging solid phase and is not segregated before the solidification front [34,35]. Michna reports that the distribution coefficient k_0 for Zr is 2.3 (for comparison, Ti has $k_0 = 7.8$) [36]. An equally important parameter for expressing the effectiveness of a chemical element used as an inoculant is the growth restriction factor Q . A higher value of the Q [K] factor means that the grain refiner element more effectively

restricts grain growth and affects the formation of a fine-grained equiaxed structure [37]. Wang calculated that the Q factor of Zr in Al acquired a value of only 1 K (Ti has value of $Q = 0$ K). Wang explains the high efficiency of grain refinement using Zr, even in the case of a low Q value, according to the particle sizes of the nuclei. The refining effect of Zr is induced by the size of the intermetallic phases of Al_3Zr , because, as defined by the theory of free growth, the larger the nuclei particles, the less undercooling is required to activate grain growth on nuclei particles. Crystallization starts preferentially on the largest nuclei particles and then gradually continues on the smaller ones [22].

3.3. Dendrite Coherency Temperature (DCT)

Dendritic crystals in an aluminum alloy split and float freely in the melt during the early stages of solidification. A coherent dendritic network is formed as the dendritic arms of the growing crystals collide as they continue to cool. The dendritic coherence temperature (DCT) is the temperature at which this phenomenon occurs. Based on an average of three measurements, the DCT temperature values for the alloys considered here are shown in Table 3. It is at this temperature that the transition from “mass” feeding to interdendritic feeding occurs, making it a critical aspect of the solidification process [38]. Numerous studies claim that casting defects such as shrinkage porosity, hot tearing, and macrosegregation begin to appear after the T_{DCP} (temperature of dendrite coherency point) is reached [39,40]. An exemplary DCT identification is shown in Figure 6, where the area with the minimum ΔT for the selected sample measurement is 0, with 0.10 and 0.20 wt.% Zr in the AlSi5Cu2Mg alloy.

Table 3. Dendritic coherence temperatures of the experimental AlSi5Cu2Mg alloy with the addition of Zr.

Zr Addition (wt.%)	0	0.05	0.10	0.15	0.20
DCT	608	610	612	613	613

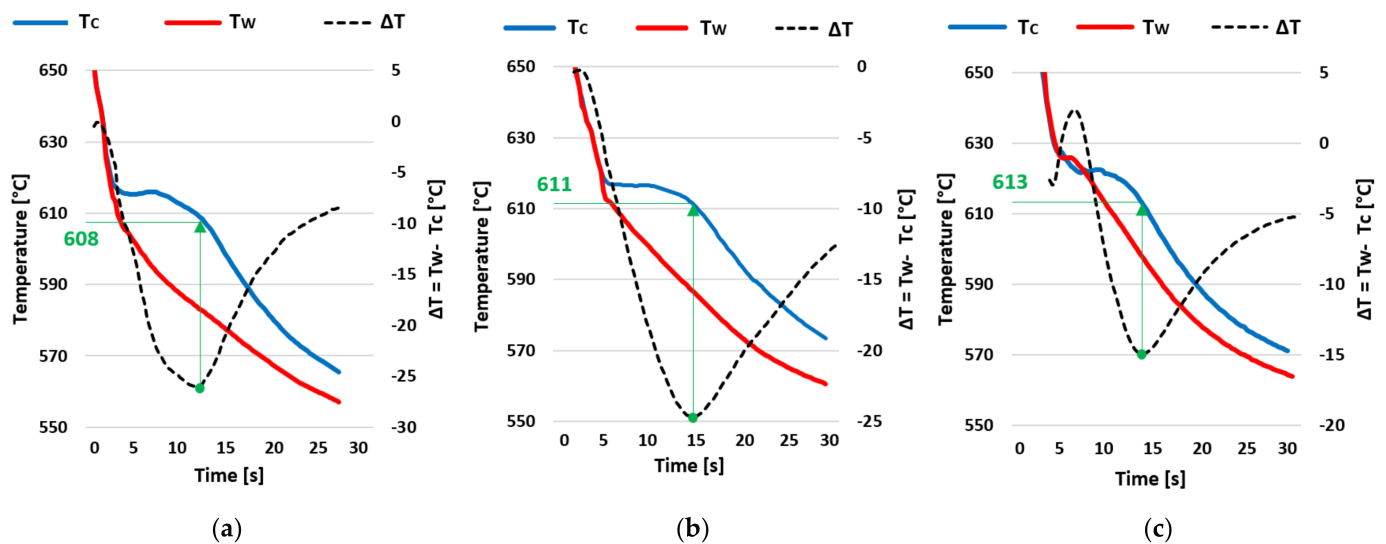


Figure 6. Identifying the DCT depending on the time and temperature difference ΔT for the experimental AlSi5Cu2Mg alloy: (a) 0 wt.% Zr (without addition); (b) addition of 0.10 wt.% Zr; (c) addition of 0.20 wt.% Zr.

The DCT for the AlSi5Cu2Mg alloy without added Zr is 608 °C. Adding 0.20 wt.% Zr to the alloy resulted in a slight increase in the DCT, to a value of 613 °C. Based on Table 3, it can be concluded that the first two increases of 0.05 wt.% Zr in the alloy resulted in an increase in the DCT of 2 °C and a third increase in an increase of 1 °C; a final increase of 0.05 wt.% Zr in the alloy had no effect on the DCT value.

Data from the literature indicate that the number of alloying elements present in the melt and the local cooling rates both have a major influence on the size of secondary dendritic arms. The effect of local cooling rates has been extensively studied; dendritic size decreases with increasing cooling rates and vice versa. Since the alloying elements are not uniformly distributed in the liquid and solid phases, their effect on the size of the dendritic arm spacing must also be considered. The volume of solute between already-formed dendritic arms increases as too much solute is pushed into the melt and away from the solidification interface. Another factor that promotes dendrite formation is the resulting constitutional undercooling or supersaturation. The distance between the main α -aluminum dendrites must be increased to make room for more solute elements. Higher concentrations of alloying elements will slow the growth of secondary dendrites and delay their contact cohesion at lower temperatures [39].

On the other hand, as mentioned above, the addition of Zr resulted in the preferential formation of intermetallic phases rich in Zr, which acted as strong nucleants for Al, so that we observed only the minimal expansion of the spaces between the primary α -aluminum dendrites for the excess number of dissolved elements. The addition of Zr also resulted in an increase in T_{liq} (Table 2), which could have a direct effect on the increase in the DCT temperature [39]. The results obtained are consistent with the research of Gómez [41], who found that a smaller grain size results in more dendrites during the solidification process. This allows the tips of the dendrites to touch each other more quickly, increasing the T_{DCP} value.

3.4. Microhardness

The microhardness of the primary α -phase of the reference alloy reached a value of 117 HM 10 (Figure 7). By adding a graded amount of Zr to the alloy, an increase in the microhardness of the primary α -phase occurred in all cases. The highest value of microhardness was achieved by the alloy with 0.10 wt.% Zr, which represents an 8% increase. However, based on the measured microhardness values, it can be argued that the amount of Zr in the alloys had only a minimal effect, since the microhardness values of the alloys containing Zr ranged from 123 to 127 HM 10.

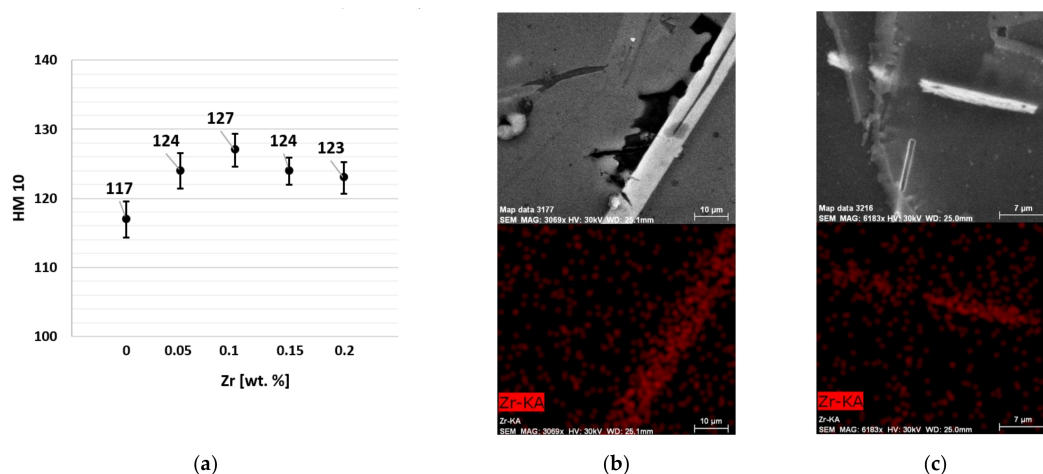


Figure 7. (a) Graphic evaluation of microhardness of experimental AlSi5Cu2Mg alloys with graded amounts of Zr according to Hamemann; (b) SEM mapping of the AlSi5Cu2Mg alloy with the addition of 0.10 wt.% Zr; (c) SEM mapping of the AlSi5Cu2Mg alloy with the addition of 0.20 wt.% Zr.

The increase in the microhardness of the primary α -phase can be attributed to two factors. The addition of Zr caused a reduction in the grains, which resulted in a larger number of grain boundaries in a given volume of material. These grain boundaries act as barriers that limit the movement of dislocations, which are responsible for the plastic deformation of the material; this has a significant effect on the microhardness of aluminum

alloys. Grain boundaries not only prevent the movement of dislocations, but also strengthen the crystal lattice around these boundaries. This strengthening effect leads to an increase in the strength of the material, as indicated by the increased microhardness [42–44]. The second factor is the presence of Zr itself in the aluminum matrix (and probably also in the substructure, as demonstrated by our previous research [45]), because Zr is characterized by high hardness [25]. Figure 7b,c shows the presence and uniform distribution of Zr in the aluminum matrix.

4. Conclusions

The present study focuses on the evaluation of the influence of graded amounts of Zr as a grain refiner element in the experimental AlSi5Cu2Mg alloy. The following conclusions can be drawn from the obtained results:

1. Due to the addition of Zr in amounts ranging from 0.05 to 0.20 wt.% into the AlSi5Cu2Mg alloy, the crystallization of Zr-based phases occurred in the form of $(Al, Si)_3Zr$ or $(Al, Si)_3(Zr, Ti)$, with a crystal structure of the DO_{22} type. These phases were observed to have a needle-faced morphology with an average length of 16.5 μm . With the addition of increasing amounts of Zr, the number of needles present in the microstructure increased, but their morphology and length did not change.
2. Newly formed intermetallic phases based on Zr acted as strong nucleation particles for α -Al grain growth in the AlSi5Cu2Mg alloy. As the amount of Zr added to the alloy increased, the inoculation effect also increased. With the addition of 0.20 wt.% Zr, grain reduction occurred by up to 53% compared to the alloy without inoculation. Grain refinement in the AlSi5Cu2Mg alloy led to an increase in the number of grain boundaries that limit the movement of dislocations, as demonstrated by an increase in the microhardness of the α -Al grains.
3. The main grain-refining effect can be attributed to the particle size of Zr-based nucleants. With the increase in the number of sufficiently large Zr-based nucleates, less undercooling was required for primary grain growth on the nucleating particles, which is consistent with the theory of free growth.
4. The evaluation of the crystallization process pointed to a gradual increase in the temperature of the liquidus and the associated expansion of the solidification interval of the AlSi5Cu2Mg alloy due to the increase in the amount of wt.% Zr in the alloy. For an alloy with 0.20 wt.% Zr, the temperature of the liquidus was 7 °C higher than that of the AlSi5Cu2Mg alloy without the addition of Zr. By gradually increasing the addition of Zr to the AlSi5Cu2Mg alloy, the dendrite coherence temperature (DCT) also gradually increased. A temperature rise of 5 °C occurred between the AlSi5Cu2Mg alloy without added Zr and the alloy with the addition of 0.20 wt.% Zr.
5. The addition of Zr to the AlSi5Cu2Mg alloy provided benefits in the form of the grain refinement of the α -Al phase and the positive outcomes associated with this phenomenon. The addition of 0.20 wt.% Zr proved to be the ideal amount.

Author Contributions: Conceptualization, D.B. and M.M.; methodology, M.M., L.Š. and M.Š.; software, M.M. and M.Š.; validation, D.B., M.M. and L.Š.; formal analysis, M.M. and L.Š.; investigation, M.M. and M.Š.; resources, D.B. and L.Š.; data curation, M.M. and M.Š.; writing—original draft preparation, M.M. and L.Š.; writing—review and editing, D.B. and M.M.; visualization, M.M., L.Š. and M.Š.; supervision, D.B. and M.M.; project administration, D.B.; funding acquisition, D.B. All authors have read and agreed to the published version of the manuscript.

Funding: This research was created within the project of the grant agency VEGA 1/0160/22 and KEGA 029ŽU-4/2023. The authors thank for the support.

Data Availability Statement: The raw data supporting the conclusions of this article will be made available by the authors on request.

Conflicts of Interest: The authors declare no conflict of interest.

References

1. Medlen, D.; Bolibruchová, D. The Influence of Remelting on the Properties of AlSi6Cu4 Alloy Modified by Antimony. *Arch. Foundry Eng.* **2021**, *12*, 81–86. [[CrossRef](#)]
2. Czerwinski, F.; Emadi, D.; Sediako, D.G.; Shaha, S.K. High-Temperature Aluminum Alloys for Automotive Powertrain. *Adv. Mater. Process.* **2016**, *174*, 16–20. [[CrossRef](#)]
3. Bruna, M.; Remisová, A.; Sládek, A. Effect of Filter Thickness on Reoxidation and Mechanical Properties of Aluminium Alloy AlSi7Mg0.3. *Arch. Metall. Mater.* **2019**, *64*, 1100–1106. [[CrossRef](#)]
4. Sigworth, G.; Campbell, J.; Jorstad, J. The Modification of Al-Si Casting Alloys: Important Practical and Theoretical Aspects. *Int. J. Met.* **2009**, *3*, 65–78. [[CrossRef](#)]
5. Lei, Z.; Wen, S.; Huang, H.; Wei, W.; Nie, Z. Grain Refinement of Aluminum and Aluminum Alloys by Sc and Zr. *Metals* **2023**, *13*, 751. [[CrossRef](#)]
6. Rath, S.K.; Sharma, A.; Sabatino, M.D. Grain Refinement of Al-Si Alloys: Scientific and Industrial Aspects. *J. Mod. Thermodyn. Mech. Syst.* **2019**, *1*, 7–15.
7. Dong, X.; Amirkhanlou, S.; Ji, S. Formation of strength platform in cast Al-Si-Mg-Cu alloys. *Sci. Rep.* **2019**, *9*, 9582. [[CrossRef](#)] [[PubMed](#)]
8. Farkoosh, A.R.; Chen, X.G.; Pegguleryuz, M. Dispersoid strengthening of a high temperature Al-Si-Cu-Mg alloy via Mo addition. *Mater. Sci. Eng.* **2015**, *620*, 181–189. [[CrossRef](#)]
9. Zhang, B.; Zhang, L.; Wang, Z.; Gao, A. Achievement of High Strength and Ductility in Al-Si-Cu-Mg Alloys by Intermediate Phase Optimization in As-Cast and Heat Treatment Conditions. *Materials* **2020**, *13*, 647. [[CrossRef](#)] [[PubMed](#)]
10. Samuel, E.; Tahiri, H.; Samuel, A.M.; Songmene, V.; Samuel, F.H. *A Review on Fundamentals of Grain Refining of Al-Si Cast Alloys*; IntechOpen: London, UK, 2024. [[CrossRef](#)]
11. Samuel, A.M.; Samuel, E.; Songmene, V.; Samuel, F.H. A Comparative Study of Grain Refining of Al-(7–17%) Si Cast Alloys Using Al-10% Ti and Al-4% B Master Alloys. *Materials* **2023**, *16*, 2867. [[CrossRef](#)]
12. Ait El Haj, B.; Hamadallah, A.; Bouayad, A.; El Akili, C. Review of Grain Refinement Performance of Aluminium Cast Alloys. *Metall. Mater. Eng.* **2023**, *29*, 1–15. [[CrossRef](#)]
13. Xie, H.; Lv, J. Precipitation of TiAl₃ in remelting Al-5Ti-1B and the grain refinement of 7050 alloy. *Mater. Res. Express* **2024**, *8*, 066513. [[CrossRef](#)]
14. Xu, C.; Xiao, W.L.; Wen, S.Z.; Zhen, Y.J.; Ma, C.L. Microstructures and grain refinement performance of Al-Ti-B-C grain refiner via powder metallurgy. *Rare Met.* **2022**, *41*, 2357–2362. [[CrossRef](#)]
15. Choudhary, C.; Bar, H.N.; Pramanick, A.K.; Sahoo, K.L.; Mandal, D. Effect of Strain Induced Melt Activation Process on the Microstructure and Mechanical Properties of Al-5Ti-1B Treated Al-7Si Alloy. *Met. Mater. Int.* **2022**, *28*, 2529–2542. [[CrossRef](#)]
16. Chen, Z.; Yan, K. Grain refinement of commercially pure aluminum with addition of Ti and Zr elements based on crystallography orientation. *Sci. Rep.* **2020**, *10*, 16591. [[CrossRef](#)] [[PubMed](#)]
17. Kelly, P.M.; Zhang, M.X. *Edge-to-Edge Matching—A New Approach to the Morphology and Crystallography of Precipitates*; The University of Queensland: Brisbane, QLD, Australia, 1999; pp. 41–62.
18. Samuel, E.; Samuel, A.M.; Songmene, V.; Samuel, F.H. A Review on the Analysis of Thermal and Thermodynamic Aspects of Grain Refinement of Aluminum-Silicon-Based Alloys. *Materials* **2023**, *16*, 5639. [[CrossRef](#)]
19. Sujith, S.V.; Kim, H.; Mulik, R.S.; Park, H.; Lee, J. Synergistic Effect of In-Situ Al-7075/Al₃Ti Metal Matrix Composites Prepared via Stir-Assisted Ultrasonic Melt Processing Under Dynamic Nucleation. *Met. Mater. Int.* **2022**, *28*, 2288–2303. [[CrossRef](#)]
20. Mao, G.; Tong, G.; Gao, W.; Liu, S.; Zhong, L. The poisoning effect of Sc or Zr in grain refinement of Al-Si-Mg alloy with Al-Ti-B. *Mater. Lett.* **2021**, *301*, 130428. [[CrossRef](#)]
21. Wang, F.; Qiu, D.; Liu, Z.L.; Taylor, J.A.; Easton, M.A.; Zhang, M.X. The grain refinement mechanism of cast aluminium by zirconium. *Acta Mater.* **2013**, *61*, 5636–5645. [[CrossRef](#)]
22. Wang, F.; Qiu, D.; Liu, Z.L.; Taylor, J.; Easton, M.; Zhang, M.X. Crystallographic study of Al₃Zr and Al₃Nb as grain refiners for Al alloys. *Trans. Nonferrous Met. Soc. China* **2014**, *24*, 2034–2040. [[CrossRef](#)]
23. Jia, Z.H.; Couzinié, J.-P.; Cherdoudi, N.; Guillot, I.; Arnberg, L.; Asholt, P.; Brusethaug, S.; Barlas, B.; Massinin, D. Precipitation behaviour of Al₃Zr precipitate in Al-Cu-Zr and Al-Cu-Zr-Ti-V alloys. *Trans. Nonferrous Met. Soc. China* **2012**, *22*, 1860–1865. [[CrossRef](#)]
24. Tang, H.; Geng, Y.; Luo, J.; Xu, J.; Ju, H.; Yu, L. Mechanical Properties of High Mg-Content Al-Mg-Sc-Zr Alloy Fabricated by Selective Laser Melting. *Met. Mater. Int.* **2021**, *27*, 2592–2599. [[CrossRef](#)]
25. Vončina, M.; Kores, S.; Ernecl, M.; Medved, J. The role of Zr and T6 heat treatment on microstructure evolution and hardness of AlSi₉Cu₃(Fe) diecasting alloy. *J. Min. Metall. Sect. B-Metal.* **2017**, *53*, 423–428. [[CrossRef](#)]
26. Rahimian, M.; Amirkhanlou, S.; Blake, P.; Ji, S. Nanoscale Zr-containing precipitates; a solution for significant improvement of high-temperature strength in Al-Si-Cu-Mg alloys. *Mater. Sci. Eng. A* **2018**, *721*, 328–338. [[CrossRef](#)]
27. Samuel, E.; Nabawy, A.M.; Samuel, A.M.; Doty, H.W.; Songmene, V.; Samuel, F.H. Effect of Zr and Ti Addition and Aging Treatment on the Microstructure and Tensile Properties of Al-2%Cu-Based Alloys. *Materials* **2022**, *15*, 4511. [[CrossRef](#)] [[PubMed](#)]
28. Zhang, J.; Zeng, H.; Wang, C.; Tang, Z. Effect of Al₃Zr Dispersoid on Microstructure and Mechanical Properties of Al-Cu-Li Alloy During Composite Spinning-Extrusion Forming. *Front. Mater.* **2022**, *9*, 822589. [[CrossRef](#)]

29. Pan, S.; Qian, F.; Li, C.; Wang, Z.; Li, Y. Synergistic strengthening by nano-sized α -Al(Mn,Fe)Si and Al₃Zr dispersoids in a heat-resistant Al–Mn–Fe–Si–Zr alloy. *Mater. Sci. Eng. A* **2021**, *819*, 141460. [[CrossRef](#)]
30. Kong, Y.; Pu, Q.; Jia, Z.; Liu, M.; Roven, H.J.; Jia, J.; Liu, Q. Microstructure and property evolution of Al-0.4Fe-0.15Zr-0.25Er alloy processed by high pressure torsion. *J. Alloys Compd.* **2020**, *824*, 153949. [[CrossRef](#)]
31. Backerud, S.L.; Sigworth, G.K. Recent Developments in the Thermal. Analysis of Aluminum Casting Alloys. *AFS Trans.* **1989**, *97*, 459–464.
32. Kaiser, M.; Rashed, M. Precipitation behavior prior to hot roll in the cold-rolled Al-Mg and Al-Mg-Zr alloys. *Met. Mater.* **2022**, *60*, 247–256. [[CrossRef](#)]
33. Bolibruchová, D.; Sýkorová, M.; Brůna, M.; Matejka, M.; Širanec, L. Effect of Zr Addition on Selected Properties and Microstructure of Aluminum Alloy AlSi5Cu2Mg. *Inter. J. Metalcast.* **2023**, *17*, 2598–2611. [[CrossRef](#)]
34. Campbell, J. Complete Casting Handbook. In *Metal Casting Processes, Metallurgy, Techniques and Design*, 2nd ed.; Butterworth-Heinemann: Oxford, UK, 2015; p. 1141.
35. Hernandez-Sandoval, J.; Garza-Elizondo, G.H.; Samuel, A.M.; Valtierra, S.; Samuel, F.H. The ambient and high temperature deformation behavior of Al–Si–Cu–Mg alloy with minor Ti, Zr, Ni additions. *Mater. Des.* **2014**, *58*, 89–101. [[CrossRef](#)]
36. Michna, Š. *Encyclopedia of Aluminum*; Adin s.r.o.: Prešov, Slovakia, 2014; p. 700. (In Czech)
37. Chen, Z.; He, Z.; Jie, W. Growth restriction effects during solidification of aluminium alloys. *Trans. Nonferrous Met. Soc. China* **2008**, *19*, 410–413. [[CrossRef](#)]
38. Djurdjevic, M.B.; Byczynski, G. The impact of chemistry on the dendrite coherency point of the 3XX series of Al alloys. In Proceedings of the ICAA_11, Aachen, Germany, 22–26 September 2008; Volume 1, pp. 1–12.
39. Chai, G.; Backerud, L.; Rolland, T.; Arnberg, L. Dendrite Coherency during Equiaxed Solidification in Binary Aluminum Alloys. *Met. Trans. A* **1995**, *26*, 965–970. [[CrossRef](#)]
40. Huber, G.; Djurdjevic, M.B.; Manasijević, S. *Quantification of Feeding Regions of Hypoeutectic Al-(5, 7, 9)Si-(0-4)Cu (wt.%) Alloys Using Cooling Curve Analysis*; IntechOpen: London, UK, 2020. [[CrossRef](#)]
41. Gómez, I.V.; Viteri, E.V.; Montero, J.; Djurdjevic, M.; Huber, G. The Determination of Dendrite Coherency Point Characteristics Using Three New Methods for Aluminum Alloys. *Appl. Sci.* **2018**, *8*, 1236. [[CrossRef](#)]
42. Pan, H.; He, Y.; Zhang, X. Interactions between Dislocations and Boundaries during Deformation. *Materials* **2021**, *14*, 1012. [[CrossRef](#)] [[PubMed](#)]
43. Lanjewar, H.; Kestens, L.A.I.; Verleysen, P. Damage and strengthening mechanisms in severely deformed commercially pure Al: Experiments and modeling. *Mater. Sci. Eng. A* **2021**, *800*, 140224. [[CrossRef](#)]
44. Shaokun, T.; Jingyuan, L.; Junlong, Z.; Zhumabieke, W.; Dan, L. Effect of Zr and Sc on microstructure and properties of 7136 aluminum alloy. *J. Mater. Res. Technol.* **2019**, *8*, 130–140. [[CrossRef](#)]
45. Bolibruchová, D.; Matejka, M.; Brůna, M.; Kuriš, M.; Michalcová, A. Investigation of Microstructure and Mechanical Properties of AlSi7Mg0.3Cu0.5 Alloy with Addition of Zr, Ti and Sr. *Inter. J. Metalcast.* **2023**, *17*, 2584–2597. [[CrossRef](#)]

Disclaimer/Publisher’s Note: The statements, opinions and data contained in all publications are solely those of the individual author(s) and contributor(s) and not of MDPI and/or the editor(s). MDPI and/or the editor(s) disclaim responsibility for any injury to people or property resulting from any ideas, methods, instructions or products referred to in the content.